INTERNATIONAL JOURNAL OF HYDROGEN ENERGY 39 (2014) 8675–8681

Available online at www.sciencedirect.com

ScienceDirect

journal homepage: www.elsevier.com/locate/he

Cu/MnO_x–CeO_2 and Ni/MnO_x–CeO_2 catalysts for the water–gas shift reaction: Metal–support interaction

Eduardo Poggio-Fraccari [a,*], *Jorge Sambeth* [b], *Graciela Baronetti* [a], *Fernando Mariño* [a]

[a] *Laboratorio de Procesos Catalíticos, DIQ-FIUBA, Universidad de Buenos Aires, Pabellón de Industrias, Ciudad Universitaria, 1428 Buenos Aires, Argentina*

[b] *CINDECA, CCT CONICET La Plata, Facultad de Ciencias Exactas, UNLP, La Plata, Argentina*

ARTICLE INFO

Article history:
Received 16 August 2013
Accepted 6 December 2013
Available online 4 January 2014

Keywords:
Hydrogen purification
Fuel cells
Ilmenite
Spinel
Cerium
Manganese

ABSTRACT

Monometallic copper and nickel catalysts supported on cerium-manganese mixed oxides are prepared, characterized and evaluated for the Water–Gas Shift (WGS) reaction. Active metal loading of 2.5 wt% and 7.5 wt% are used to impregnate MnO_x–CeO_2 supports with 30% and 50% Mn:Ce molar ratio. The structure of the samples strongly depends on both the active metal employed and the manganese content in the mixed support. For both Cu and Ni samples, the best catalytic behavior is found in samples supported on the MnO_x–CeO_2 oxides with 30% Mn:Ce molar ratio, as a result of the presence of $Cu_xMn_yO_4$ spinel-type phases in the case of copper catalysts and the presence of a $NiMnO_3$ mixed oxide with defect ilmenite structure in the case of nickel catalysts.

1. Introduction

Hydrogen is the ideal fuel to feed low-temperature PEM fuel cells (PEMFC) used in mobile sources. Noble metal based PEMFC anodes require a CO concentration in the inlet gas lower than 10–20 ppm. Otherwise, the anode is poisoned. When H_2 is produced from carbon containing molecules (hydrocarbons or alcohols), a purification process is required to reduce CO levels to cell tolerance. Considering the purification route proposed by Zalc and Löffler [1], Water–gas Shift (WGS) converter is expected to have the largest volume since the intrinsic activity of commercial catalysts is low [2–4]. The new application of H_2 in fuel cells for mobile sources has renewed the interest in the study of WGS catalysts. The requirements of WGS catalysts for fuel cell applications are quite different from those of the catalysts currently used in chemical plants. The catalyst bed must have a reduced volume and weight and catalysts must retain an acceptable activity after many start-up and shut-down cycles. In addition, the catalyst must not require complex pretreatment procedures and they must be non-pyrophoric and oxidation-tolerant on exposure to air [5,6].

* *Corresponding author*. Laboratorio de Procesos Catalíticos, Departamento de Ingeniería Química, Facultad de Ingeniería, Universidad de Buenos Aires, Pabellón de Industrias, Ciudad Universitaria, 1428 Buenos Aires, Argentina. Tel.: +54 11 45763240; fax: +54 11 45763241.
E-mail address: eduardoaristidespf@di.fcen.uba.ar (E. Poggio-Fraccari).

0360-3199/$ – see front matter
http://dx.doi.org/10.1016/j.ijhydene.2013.12.063

There is evidence that the support has a significant effect on the overall catalytic behavior in oxidation reactions such as low-temperature CO oxidation or WGS reaction [7]. The use of active oxides as support, like ceria-based oxides, results in superior activity compared to catalysts supported on other oxides, such as Al_2O_3 or SiO_2. In fact, earlier works have shown that the ability of the metal oxide used as support to undergo redox cycles is crucial for the activity [8]. Furthermore, the catalytic performance of such oxides is notably improved by the addition of even small amounts of transition metals (Co, Cr, Cu, Ni), which are able to enhance oxygen storage capacity and surface mobility [8–10].

In a previous work [11], we have shown that the activity of cerium-manganese mixed oxides for the WGS reaction is markedly higher than that of pure CeO_2 or MnO_x in the temperature range 400–450 °C. The superior catalytic behavior of Mn–Ce samples can be explained from a combination of two effects: a greater reducibility of manganese species and a higher surface area of mixed samples with respect to pure manganese oxide. In that work, it was also observed that impregnation of MnO_x–CeO_2 oxides with transition metals such as copper or nickel results in superior WGS catalysts compared to the corresponding bare supports.

2. Experimental

Manganese-cerium mixed oxides support precursors were prepared by co-precipitation technique from aqueous solutions of metallic salts $Ce(NO_3)_3$ 0.1 M and $Mn(NO_3)_2{\cdot}4H_2O$ 2 M in basic medium at room temperature, using NaOH 3 M as precipitant agent [12]. After precipitation, precursors were washed with bi-distilled water up to the presence of Na cations is not further detected. Then, they were dried at 100 °C and calcined at 450 °C in air for 5 h. Supports with Mn/Ce molar ratio of 30 and 50 were prepared, thereafter called CeMn30 and CeMn50, respectively.

CeMn30 and CeMn50 support samples were impregnated for 5 h at room temperature with Cu^{2+} or Ni^{2+} salts ($Cu(NO_3)_2{\cdot}3H_2O$ or $Ni(NO_3)_2.6H_2O$), in order to obtain copper and nickel monometallic catalysts [13]. Then, the slurry was filtered, dried overnight at 70 °C and calcined in the same conditions and procedure as used the MnO_x–CeO_2 supports. Catalysts with Cu or Ni content of 2.5 and 7.5 wt% over both MnO_x–CeO_2 supports were prepared.

Solids were also analyzed by X-ray Diffraction (XRD) in a Philips PW 1390 equipment with radiation corresponding to CuKα. Data was collected in steps of 0.02° (2θ) with a fixed-time counting of 1 s. Temperature-programmed reduction experiments were performed in a Micromeritics Autochem II 2920 apparatus coupled to mass spectrometer Thermostar Pfeiffer using a 50 ml/min stream with 4% of H_2 (in Ar) and a sample mass of 30 mg. Temperature was raised from RT to 600 °C, following a temperature ramp of 10 °C/min. Prior to TPR experiments, all samples was preheated in air (air flow = 100 ml/min, temperature = 450 °C) during 60 min in order to clean the surface. Then, the samples were cooled to RT and purged with Ar, before starting the TPR experiment.

WGS activity tests were conducted in an isothermal fixed bed glass reactor heated with an electrical oven. Catalytic performance was evaluated at several temperatures in the range 250–450 °C. In a typical test, 120 mg of catalyst and a total inlet flow of 150 ml/min, with 8% of CO, 24% H_2O, 45% H_2, and N_2 as balance, were employed. Before each catalytic run, solids were reduced in-situ during 30 min with an H_2 stream (50% of H_2 in N_2) at the higher temperature of reaction (450 °C). At the reactor outlet, analysis of non-converted CO and gaseous products was performed by a Hewlett Packard HP 6890 gas chromatograph equipped with a TCD detector. CO conversion is conventionally defined by Eq. (1).

$$x = \frac{F_{CO}^{in} - F_{CO}^{out}}{F_{CO}^{in}} \quad (1)$$

Considering that methanation reaction could occur, conversion towards CO_2 is defined through Eq. (2).

$$x_{CO_2} = \frac{F_{CO_2}^{out}}{F_{CO}^{in}} \quad (2)$$

where F_i^{in} and F_i^{out} are the inlet and outlet molar flow of gas i, respectively. Reported values of CO conversion and CO_2 conversion correspond to steady state values.

3. Results and discussion

XRD patterns of monometallic Cu and Ni catalysts supported on CeMn30 and CeMn50 are presented in Figs. 1–4. Fig. 1 shows that the diffraction lines corresponding to $NiMnO_3$ phase (#752089) are found for both nickel catalysts studied (2.5Ni/CeMn30 and 7.5Ni/CeMn30 samples). These diffraction lines are not present in the patterns of nickel catalysts supported on CeMn50 (Fig. 2). However, segregation of NiO phase (#780643) is detected in both 2.5Ni/CeMn50 and 7.5Ni/CeMn50 samples.

Concerning to XRD patterns of copper-containing samples shown in Figs. 3 and 4, diffraction peaks of a spinel-type $Cu_xMn_yO_4$ phase are observed in all the copper catalysts studied. Although signals of $Cu_xMn_yO_4$ are partially superimposed to MnO_x reflections in the case of catalysts supported

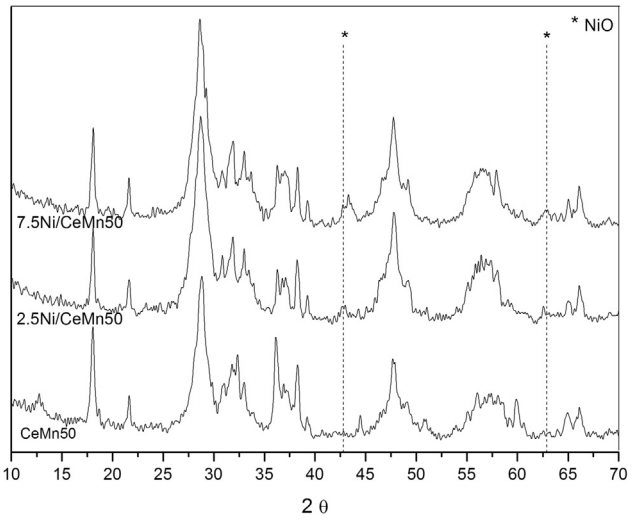

Fig. 1 – XRD patterns of Ni/CeMn50 catalysts.

on CeMn50 (Fig. 4), the presence of the spinel-type phases in these catalysts can be inferred by the presence a $Cu_xMn_yO_4$ reflection at $2\theta = 35.7°$. Besides, the characteristic reflections of a segregated CuO phase (#780428) are only found for copper catalysts supported on CeMn50 (Fig. 4).

Comparison of the diffraction patterns of Ni (Fig. 1) or Cu catalysts (Fig. 3) supported on CeMn30 with that of the bare support reveals that the structure of the Mn–Ce mixed oxide drastically changes. Indeed, reflections of MnO_x phases ($2\theta = 18.1$, 21.3, 31.8° and others) are visible in the case of CeMn30 support, but they disappear in the patterns of Cu/CeMn30 catalysts. On the contrary in Figs. 2 and 4, which correspond to catalysts supported on CeMn50, it can be observed that characteristic signals of MnO_x phases are present in both support and catalysts.

In addition, from the comparison between XRD patterns of copper catalysts and supports it is evident that characteristic peaks of the fluorite-like cubic phase of ceria become more pronounced in the case of the catalysts. XRD patterns of Cu/CeMn30 catalysts and CeMn30 support in the 2θ range from 26° to 31° are showed in Fig. 5. In the same figure, pure CeO_2 diffraction pattern is added for the sake of comparison. In a previous work, D'Alessandro et al. [12] reported that this ceria reflection shifts to the right (towards higher θ values) upon formation of MnCe solid solution. This feature could be explained by the partial substitution of a bigger cation (Ce^{4+}, ionic radii = 0.098 nm) by a smaller one (Mn^{3+}, ionic radii = 0.065 nm) into the fluorite structure of ceria [14,15].

Fig. 5 reveals that the peak located at $2\theta = 28.7°$ in the diffraction pattern of the Mn–Ce bare oxides shifts approximately 0.10° towards lower 2θ values in the case of copper catalysts. Similarly to what was proposed regarding a MnO_x–CeO_2 solid solution, this shift to a lower angle might come from the substitution of Mn^{3+} by a bigger cation (Cu^{2+}, ionic radii = 0.073 nm). To sustain this interpretation, it should be mentioned that some works have reported that CuO can dissolve within CeO_2 lattice at low dopant concentrations [16,17]. However, an additional interpretation of the peak shifts in Fig. 5 arises from our XRD results previously presented for copper catalysts, where characteristic reflections of $Cu_xMn_yO_4$ spinel-type phase were found. It could be readily seen from Fig. 5 that ceria (111) signal is more intense in the catalysts than in the supports, which would indicate a lower degree of manganese substitution in the formers. As a consequence, it could be suggested that some Mn ions are removed from ceria lattice to form the spinel phase after impregnation with copper of MnO_x–CeO_2 support and the subsequent calcination procedure. Obviously, some manganese ions in the spinel phase could also come from segregated manganese oxides. XRD reflections of MnO_x are still visible in the patterns of Cu/CeMn50 catalysts but completely absent in the patterns of Cu/CeMn30 catalysts.

TPR profiles of CeMn30 and CeMn50 mixed oxides were presented in a previous work [13]. In both cases, two reduction peaks (α and β as temperature increases) are present in the temperature range 200–450 °C. Both peaks were attributed to H_2 consumption by manganese oxide species and not to cerium reduction by most of the authors [18,19]. As we have previously reported [13], these two peaks were ascribed to the step reduction of species with different Mn oxidation states. Furthermore, from the ratio between H_2 consumption in both events, it was postulated that most of the manganese in CeMn30 and CeMn50 samples is present as MnO_2 before TPR is performed, as Mn_3O_4 after peak and as MnO for temperatures higher than 450 °C (after β peak).

Fig. 6 shows the temperature-programmed reduction profiles of copper and nickel catalysts supported on CeMn30. To help the interpretation of the results, the positions of α and β peaks of CeMn30 support are included in the same figure. In the profiles of Ni catalysts, α and β consumption peaks are closer one to each other. The resulting broad event includes the step reduction of manganese oxides and the reduction of the spinel $NiMnO_3$ detected by XRD for both Ni/CeMn30 catalysts studied. The profiles of copper catalysts exhibit a broad peak in the 160–320 °C temperature range. In agreement with XRD analysis, this feature corresponds to H_2 consumption during the reduction of spinel-type phases generally named $Cu_xMn_yO_4$. It must be remarked the absence of other reduction peaks at higher temperatures, which is in good agreement

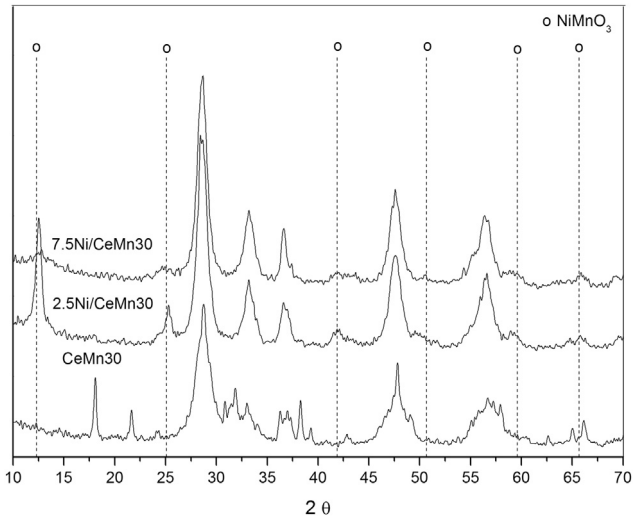

Fig. 2 – XRD patterns of Ni/CeMn30 catalysts.

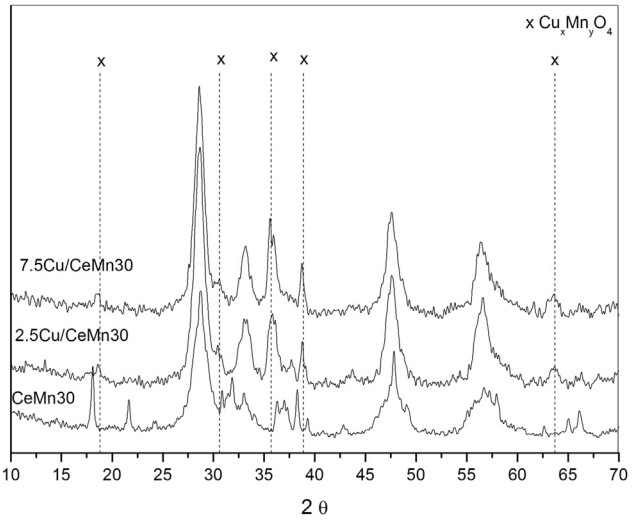

Fig. 3 – XRD patterns of Cu/CeMn30 catalysts.

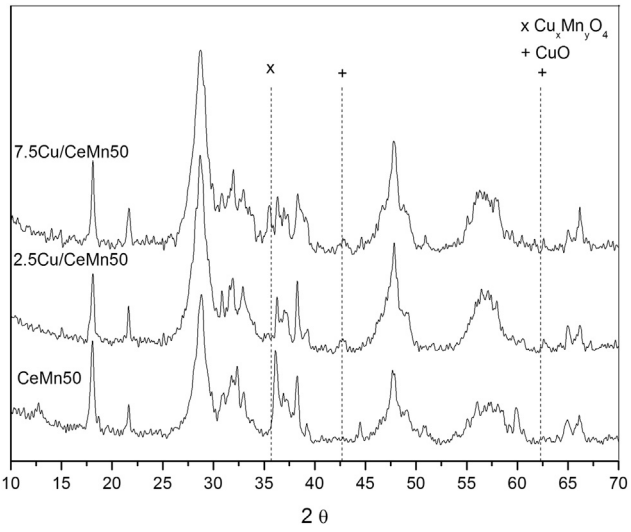

Fig. 4 – XRD patterns of Cu/CeMn50 catalysts.

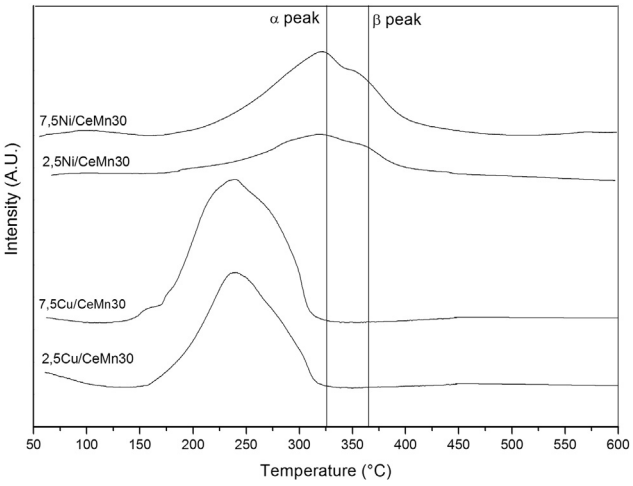

Fig. 6 – TPR of Cu/CeMn30 and Ni/CeMn30 catalysts.

with the nonappearance of MnO_x XRD reflections for these Cu/CeMn30 samples.

TPR profiles of catalysts supported on CeMn50 are displayed in Fig. 7; again, α and β peak temperatures for CeMn50 support are indicated. As it can be seen, the bimodal curve of the MnO_x–CeO_2 support is conserved in the profiles of Ni catalysts and the positions of both peaks are similar to those of the bare support. In any case, reduction temperatures of both features are lower than the temperature value found for bulk NiO reduction (ca. 400 °C) under the same operation conditions [11,20,21]. H_2 consumption during the first event increases as nickel content increases, suggesting that NiO reduction takes place in the low-temperature region. From the above, it can be concluded that nickel and manganese reduction occurs simultaneously during the low-temperature consumption peak. Reduction profiles of Cu/CeMn50 catalysts are also presented in Fig. 7. In this case, the consumption curves, which are completely different from the profile of the corresponding support, are more complex and they exhibit at least four reduction peaks. The first signal at approximately 150 °C was attributed to the reduction of finely dispersed CuO in contact with CeO_2 [22]. H_2 consumption in the second peak (located at ca. 200–210 °C) increases as copper loading of the samples also increases. $Cu_xMn_yO_4$ spinel-type phase was also detected by XRD in this sample. Considering that copper ions strongly interacting with the support require higher reduction temperatures, the reduction of $Cu_xMn_yO_4$ phase could take place simultaneously during this broad reduction event. The peaks at higher temperatures are ascribed to the step reduction of manganese oxides found by XRD. In accordance with other authors [23], the broad peak (centered at ca. 285 °C) corresponds to the reduction of MnO_2 to Mn_3O_4 (α peak) and the high-temperature reduction peak (centered at ca. 315 °C) involves the reductions of large clusters of copper oxide detected by XRD, surface CeO_2 and Mn_3O_4. As it can be seen, the reduction step Mn_3O_4 → MnO is notably favored with respect to the β peak of the bare CeMn50 support. For a similar

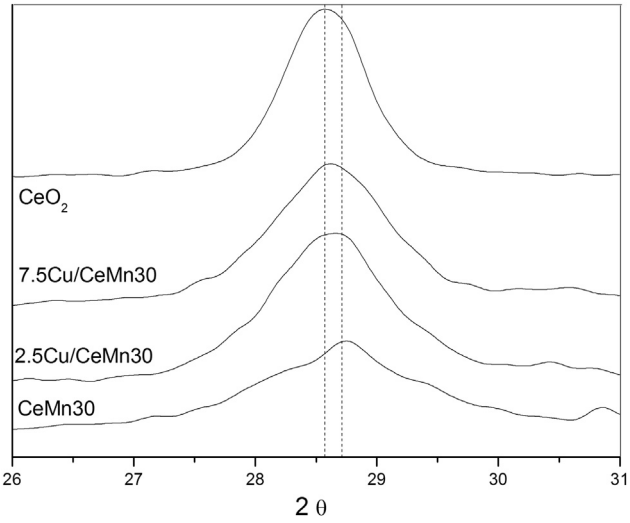

Fig. 5 – XRD patterns of (111) reflection of fluorite phase for Cu/CeMn30, catalysts, CeMn30 and CeO_2.

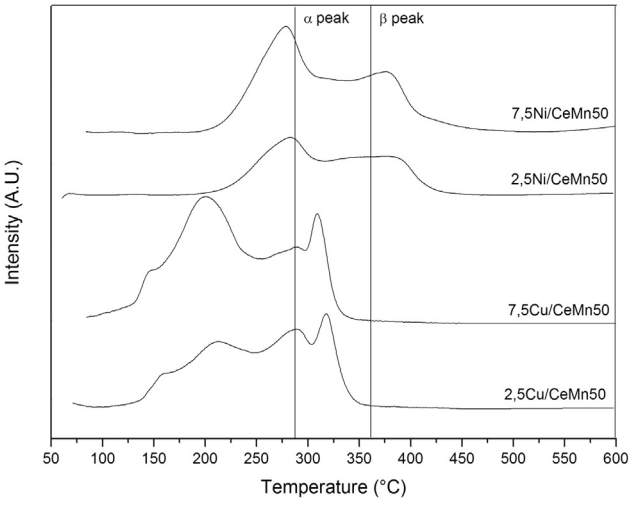

Fig. 7 – TPR of Cu/CeMn50 and Ni/CeMn50 catalysts.

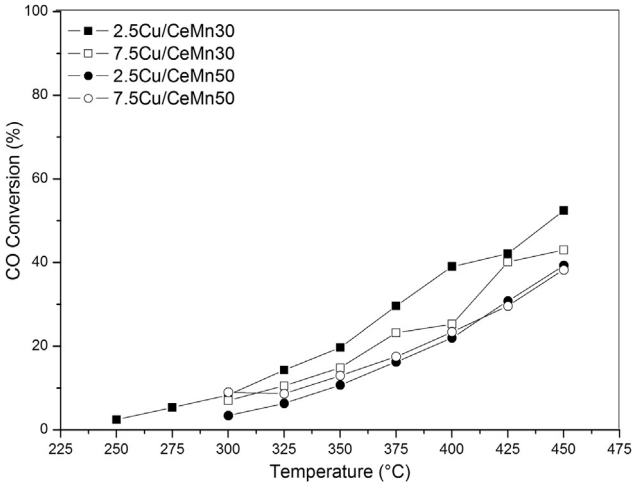

Fig. 8 – CO conversion versus temperature of copper catalysts.

Cu/MnO_x–CeO_2 catalytic system, it has been reported that the presence of copper significantly shifted the high-temperature reduction events to lower temperature regions, indicating the occurrence of metal–support interaction. This improvement was often interpreted in terms of the activation and spillover of hydrogen from the initially reduced copper to the manganese and cerium oxides [24].

Water–gas Shift activity of copper catalysts is represented in Fig. 8 in terms of CO conversion attained at the outlet of the isothermal fixed bed reactor as a function of the operating temperature. Firstly, it should be remarked that the activity of copper catalysts is considerably higher than the activity of bare CeMn30 and CeMn50 supports, which were reported in a previous work [13]. TPR profiles presented in Figs. 6 and 7 indicate that addition of copper to CeMn30 and CeMn50 supports greatly prompted the reducibility of the catalysts, which is related to their redox activity [23]. CO conversion values obtained with copper catalysts, which are far from the equilibrium conversions, increase with the reaction temperature for the four catalytic samples studied in this work. The best catalytic activity is found for catalyst is found for sample 2.5Cu/CeMn30, with a CO conversion higher than 50% at 450 °C. Nevertheless, copper loading of the catalysts has little influence on the activity of the samples. In relation to the role of the support, Fig. 8 clearly exposes that samples prepared on CeMn30 are more active than samples supported on CeMn50 for both copper loadings studied. Other authors [25] have found a correlation between the reducibility of several CuO–CeO_2 catalysts doped with transition metal oxides (ZnO, MnO_2 and Fe_2O_3) and their low temperature catalytic activity for CO oxidation reaction. Therefore, the presence of highly reducible $Cu_xMn_yO_4$ spinel-type species observed in both XRD and TPR characterizations would be responsible for the enhanced WGS activity of samples supported on CeMn30.

The activity of nickel catalysts presented in Fig. 9 evidences that Ni catalysts are more active than Cu catalysts, particularly at high temperatures and at high metal contents. Catalyst 7.5Ni/CeMn50, for example, is able to convert more than 90% of CO for temperatures higher than 380 °C. The influence of metal content is completely opposite to that previously presented for copper catalysts. As it can be observed in Fig. 9, the activity of the samples significantly increases with nickel content. With regards to support effect, the results also show the inverse trend with respect to copper samples: catalysts prepared on CeMn50 are more active than samples supported on CeMn30 for both nickel contents. However, the influence of the support is less important for the samples with low nickel content.

It was widely reported that nickel is an effective catalyst for methanation reactions [26,27]. In particular, nickel catalysts supported on ceria-based oxides have demonstrated to favor CO methanation in reformate gas [28,29]. Since the catalysts studied in this work have shown activity for methane production, it is necessary to quantify the undesired methanation occurrence. Hence, Fig. 10 presents the effective CO conversion towards CO_2 by WGS reaction, as defined by Eq. (2). From the comparison of Figs. 9 and 10, it can be inferred that total CO conversion and WGS conversion to CO_2 are coincident at

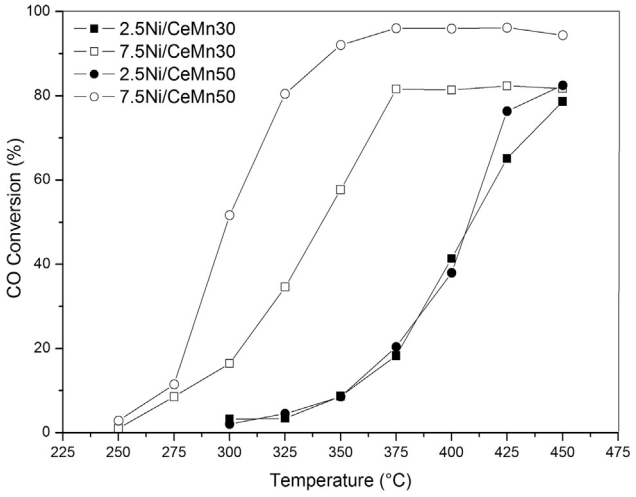

Fig. 9 – CO conversion versus temperature of nickel catalysts.

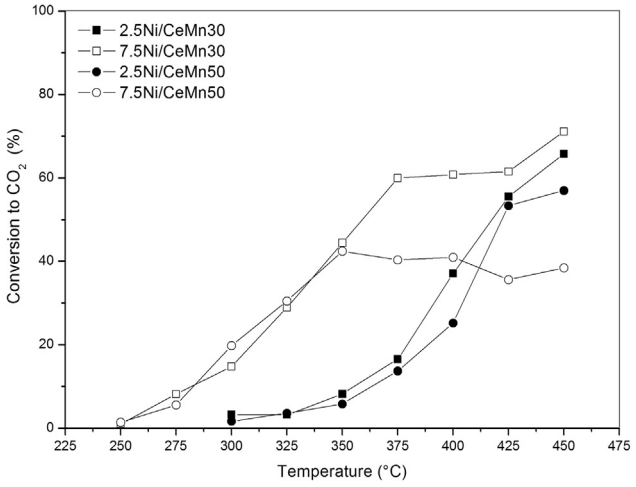

Fig. 10 – CO_2 conversion versus temperature of nickel catalysts.

low temperature. As temperature increases, methanation reaction becomes more important and both curves take different paths. Methanation starts at lower temperatures for higher nickel content catalysts. Besides, bringing into comparison catalysts with constant metal loading, methanation appears at lower temperatures for samples supported on CeMn50. Even more, the trends observed for total CO conversions (Fig. 9) are completely different in Fig. 10: (i) Ni/CeMn30 catalysts are more selective than Ni/CeMn50 samples, and (ii) WGS activity weakly depends on nickel loading of the catalysts.

Nickel particles supported on oxides are well-known catalysts for the formation of methane from CO and H_2. Then, the high methanation activity of Ni/CeMn50 catalysts can be explained by the presence of a segregated NiO phase, which was found by XRD and TPR. In addition, TPR profiles of these samples have shown that the peak assigned to NiO reduction is greater for the high Ni content catalysts. This observation is in good agreement with the enhanced methanation activity of 7.5Ni/CeMn50 catalyst.

On the contrary, catalysts supported on CeMn30 have shown the presence of a $NiMnO_3$ mixed oxide with ilmenite-like structure [30]. The improved WGS selectivity of these samples has been explained by a stronger Ni-support interaction that prevents the formation of bulk-like particles of Ni [30] and by the presence of stabilized Mn^{4+} ions in the defect ilmenite structure that improve the oxygen mobility and the redox activity of the catalysts [31,32].

4. Conclusions

Monometallic copper and nickel catalysts supported on cerium-manganese mixed oxides were prepared, characterized and evaluated for the Water–Gas Shift (WGS) reaction. The structure of the samples strongly depends on both the active metal employed and the manganese content in the mixed support. Copper catalysts supported on the low manganese content sample (CeMn30) have shown greater reducibility and higher WGS activity than copper catalysts prepared on the high manganese content support. $Cu_xMn_yO_4$ spinel-type species are identified as responsible for this improved catalytic behavior. Total CO conversion values attained with nickel catalysts supported on the high manganese content oxide (CeMn50) are greater than those of Ni/CeMn30 samples but methanation reaction, which consumes H_2 present in the feed, proceeds more readily on the formers. Consequently, Ni/CeMn30 samples exhibit superior activity for the effective WGS conversion to CO_2. The better selectivity of Ni/CeMn30 samples is ascribed to $NiMnO_3$ phase with ilmenite-like structure detected by XRD that prevents the formation of bulk-like particles of Ni and improves the oxygen mobility and the redox activity of the catalysts.

Acknowledgments

To the University of Buenos Aires (UBA), the University of La Plata (UNLP), ANPCyT and CONICET for their financial support.

REFERENCES

[1] Zalc JM, Löffler DG. Fuel processing for PEM fuel cells: transport and kinetic issues of system design. J Power Sources 2002;111:58–64.
[2] Newsome DS. Water–gas shift reaction. Catal Rev Sci Eng 1980;21:275–81.
[3] Gonzalez JC, Gonzalez MC, Laborde MA, Moreno N. Effect of temperature and reduction on the activity of high temperature water gas shift catalysts. Appl Catal 1986;20:3–13.
[4] Amadeo NE, Laborde MA. Hydrogen production from the low-temperature water–gas shift reaction: kinetics and simulation of the industrial reactor. Int J Hydrogen Energy 1995;20:949–56.
[5] Song C. Fuel processing for low temperature and high temperature fuel cells: challenges and opportunities for sustainable development in the 21st century. Catal Today 2002;77(1–2):17–49.
[6] Ratnasamy Ch, Wagner JP. Water gas shift catalysis. Catal Rev Sci Eng 2009;51:325–440.
[7] Kosmambetova GS, Moroz EM, Guralsky AV, Pakharukova VP, Boronin AL, Ivashchenko TS, et al. Low temperature hydrogen purification from CO for fuel cell application over copper–ceria catalysts supported on different oxides. Int J Hydrogen Energy 2011;36:1271–5.
[8] Mariño F, Descorme C, Duprez D. Supported base metal catalysts for the preferential oxidation of carbon monoxide in the presence of excess hydrogen (PROX). Appl Catal B Environ 2005;58:175–83.
[9] Hung C. The effect of the calcination temperature on the activity of Cu–La–Ce composite metal catalysts for the catalytic wet oxidation of ammonia solution. Powder Technol 2009;191:21–6.
[10] Chen Y, Liaw B, Chen H. Selective oxidation of CO in excess hydrogen over $CuO/Ce_xZr_{1-x}O_2$ catalysts. Int J. Hydrogen Energy 2006;31:427–35.
[11] Poggio-Fraccari E, Mariño F, Laborde M, Baronetti G. Copper and nickel catalysts supported on praseodymium-doped ceria (PDC) for the water–gas shift reaction. Appl Catal A Gen 2013;460–461:15–20.
[12] D'Alessandro O, Thomas HJ, Sambeth JE. An analysis of the first steps of phenol adsorption–oxidation over coprecipitated Mn–Ce catalysts: a DRIFTS study. React Kinet Mech Catal 2012;107:295–309.
[13] Poggio-Fraccari E, D'Alessandro O, Sambeth JE, Baronetti G, Mariño F. Ce-Mn mixed oxides as supports of Copper- and Nickel-based catalysts for water–gas shift reaction. Fuel Proc Tech 2014;119:67–73.
[14] Tikhomirov K, Kröcher O, Elsener M, Widmer M, Wokaun A. Manganese based materials for diesel exhaust SO_2 traps. Appl Catal B Environ 2006;64:160–7.
[15] Liang Q, Wu X, Weng D, Xu H. Oxygen activation on Cu/Mn–Ce mixed oxides and the role in diesel soot oxidation. Catal Today 2008;139:113–8.
[16] Lamonier C, Ponchel A, D'Huysser A, Jalowiecki-Duhame L. Studies of the cerium-metal-oxygen-hydrogen system (metal Cu, Ni). Catal Today 1999;50:247–59.
[17] Terribile D, Trovarelli A, de Leitenburg C, Primavera A, Dolcetti G. Catalytic combustion of hydrocarbons with Mn and Cu-doped ceria–zirconia solid solutions. Catal Today 1999;47:133–40.
[18] Larsson PO, Andersson A. Oxides of copper, ceria promoted copper, manganese and copper manganese on Al_2O_3 for the combustion of CO, ethyl acetate and ethanol. Appl Catal B Environ 2000;24:175–92.

[19] Hussain ST, Sayari A, Larachi F. Enhancing the stability of Mn–Ce–O WETOX catalysts using potassium. Appl Catal B Environ 2001;34:1–9.
[20] Chary K, Rao P, Vishwanathan V. Synthesis and high performance of ceria supported nickel catalysts for hydrodechlorination reaction. Catal Commun 2006;7:974–8.
[21] Xu J, Xue B, Liu YM, Li YX, Cao Y, Fan KN. Mesostructured Ni-doped ceria as an efficient catalyst for styrene synthesis by oxidative dehydrogenation of ethylbenzene. Appl Catal A Gen 2011;405:142–8.
[22] Thirupathi B, Smirniotis PG. Co-doping a metal (Cr, Fe, Co, Ni, Cu, Zn, Ce, and Zr) on Mn/TiO_2 catalyst and its effect on the selective reduction of NO with NH_3 at low-temperatures. Appl Catal B Environ 2011;110:195–206.
[23] Tang X, Xu Y, Shen W. Promoting effect of copper on the catalytic activity of MnO_x–CeO_2 mixed oxide for complete oxidation of benzene. Chem Eng J 2008;144:175–80.
[24] Tang X, Zhang B, Li Y, Xu Y, Xin Q, Shen W. CuO/CeO_2 catalysts: redox features and catalytic behaviors. Appl Catal A Gen 2005;288:116–25.
[25] Zou H, Chen S, Liu Z, Lin W. Selective CO oxidation over CuO–CeO_2 catalysts doped with transition metal oxides. Powder Technol 2011;207:238–44.
[26] Fatsikostas A, Verykios X. Reaction network of steam reforming of ethanol over Ni-based catalysts. J Catal 2004;225:439–52.
[27] Forzatti P, Lietti L. Catalyst deactivation. Catal Today 1999;52:165–81.
[28] Huang T, Yu T, Jhao S. Weighting variation of water–gas shift in steam reforming of methane over supported Ni and Ni–Cu catalysts. Ind Eng Chem Res 2006;45:150.
[29] Zyryanova MM, Snytnikov PV, Amosov YI, Kuzmin VA, Kirillov VA, Sobyanin VA. Design, scale-out, and operation of a preferential CO methanation reactor with a nickel–ceria catalyst. Chem Eng J 2011;176-177:106–13.
[30] Barrio L, Kubacka A, Zhou G, Estrella M, Martínez-Arias A, Hanson JC, et al. Unusual physical and chemical properties of Ni in $Ce_{1-x}Ni_xO_{2-y}$ oxides: structural characterization and catalytic activity for the water gas shift reaction. J Phys Chem C 2010;114:12689–97.
[31] Mehandjiev D, Zhecheva E, Ivanov G, Iancheva R. Preparation and catalytic activity of nickel–manganese oxide catalysts with an ilmenite-type structure in the reactions of complete oxidation of hydrocarbons. Appl Catal A Gen 1998;167:277–82.
[32] Zhang Y, Qin Z, Wang G, Zhu H, Dong M, Li SH, et al. Catalytic performance of MnO_x–NiO composite oxide in lean methane combustion at low temperature. Appl Catal B Environ 2013;129:172–81.